Int J Thermophys (2010) 31:1145–1156
DOI 10.1007/s10765-010-0807-8

Experimental Investigation of the Thermal Impedance of Interstitial Material at a Junction

Jianli Wang · Ming Gu · Bai Song · Xing Zhang

Received: 15 August 2009 / Accepted: 26 July 2010 / Published online: 17 August 2010

Abstract Using a quasi-steady-state T-type probe, experimental evidence of the different behavior of the thermal impedance of a junction with different interstitial material (interposer) was presented. In the T-type probe, a short hot wire serves both as a heater and a thermometer, which is subjected to an alternating current, and a thermally infinite long test wire is attached to the midpoint of the hot wire with an interposer. The thermal impedance of the interposer was introduced, which was taken to be the product of the steady-state thermal resistance and a complex ratio function. A complete expression for the thermal impedance of the interposer was derived, and the effects of the radiation heat loss as well as the deviation of the contact junction position were theoretically estimated. A microscale Pt wire with two interposers was measured, including solidified platinum black and Apiezon N vacuum grease. Experimental results showed that the platinum black contact with high thermal effusivity served as a negative thermal impedance, while a positive thermal impedance was observed for the Apiezon N contact. The obtained thermal impedance of the Apiezon N contact could be equivalent to its thermal resistance, which was verified by measuring the thermal conductivity of a Cu wire using the steady-state T-type probe.

Keywords Interstitial material · Quasi-steady-state T-type probe · Thermal effusivity · Thermal impedance

J. Wang · M. Gu · B. Song · X. Zhang (✉)
Key Laboratory for Thermal Science and Power Engineering of Ministry of Education, Department of Engineering Mechanics, Tsinghua University, Beijing 100084, China
e-mail: x-zhang@tsinghua.edu.cn

1 Introduction

When two surfaces are pressed together, due to the unevenness of the real surfaces, most of the heat passes through a limited number of actual joints, and the junction between two surfaces creates a temperature difference, thus introducing a thermal contact resistance, which is defined as

$$R = \Delta T/Q, \tag{1}$$

where ΔT is the steady-state temperature difference across the contact area and Q is the heat flow rate.

With the development of micro/nanoscale techniques, remarkable progress has been made in the area of thermometry. Since the thermal contact resistance plays a significant or even dominant role in micro/nanoscale measurements, relevant research in this area has become a hot topic [1]. A micromachined structure has been developed by Majumdar's group [2–4] to measure suspended individual nanowires. Although the thermal contact resistances between the nanowire and the two suspended sensors were estimated to be smaller than the thermal resistance of the test nanowire [2], later research observed a decrease of 9 % to 13 % of the total resistance of the nanowire after coating Pt at the contact ends [3]. Recently, the length dependence of the thermal conductivity of individual nanotubes was investigated by depositing a sequence of contacts along the test wire, and different thermal circuit models were applied to estimate the effect of the thermal contact resistance introduced by the deposition [4]. Another popular technique for thermal measurements is the 3ω method, which is widely used to measure the thermal properties of thin films and nanowires [1,5,6]. Lee et al. [5] found that the thermal conductivity of dielectric films decreased with decreasing film thickness, resulting from the interfacial thermal boundary resistance. Using the self-heating 3ω method, Wang et al. [6] reported a length dependence of the thermal conductivity of individual carbon fibers, and the thermal contact resistance was determined to be about 15 % of the total thermal resistance. Other than the above two contact methods, noncontact methods including the photothermal technique [7], thermoreflectance technique [8], and Raman spectroscopy [9] have been successfully developed to characterize the thermal interfacial resistance.

As a steady-state contact method, a T-type probe was developed to measure the thermal conductivity of micro/nanoscale wires [10–13], where the ends of a short hot wire are welded to heat sinks, and one end of the test wire is attached to the midpoint of the hot wire with an interposer. The T-type probe was first introduced by Zhang et al. [10], then was extended to measure the thermal conductivity of single carbon nanotubes [11,12]. Using this method, Fujii et al. [11] experimentally observed a diameter dependence of the thermal conductivity of carbon nanotubes, and the authors claimed that the experimental results represented the lowest bounds of the intrinsic thermal conductivity due to the presence of the thermal contact resistance between the nanotube and the metallic sensor. Dames et al. [12] deposited tungsten to the junction between the carbon nanotube and the hot wire to improve the thermal and electrical contact, but the test nanotube was contaminated with the deposition, and a reduction in the thermal contact resistance was not reported. Wang et al. [13] estimated the effect

of the thermal contact resistance at the junction between the test microscale fiber and the hot wire by changing the length of the fiber in the same contact condition at the junction. However, it is very difficult to physically change the length of the test wire, especially in the nanoscale experiment, and a stability of the operating temperature is a must in each length measurement.

Recently, based on the T-type probe, a quasi-steady-state method was developed to measure the thermal effusivity of the test wire and the thermal impedance of the junction [14], and the dynamic characteristic of the interposer was theoretically analyzed using an equivalent thermal circuit model [15]. In this article, the thermal impedances of the junction with two different interposers were measured. Experimental tests confirm that, if the interposer with a relatively low thermal effusivity is used, the dynamic thermal impedance can be equivalent to the thermal contact resistance, and the present method can be conveniently extended to nanoscale thermal characterization measurements.

2 Theoretical

2.1 Physical Model

In the self-heating 3ω method, as shown in Fig. 1a, a metallic hot wire serves both as a thermometer and a heater, which is supported by two heat sinks. If an alternating current, $I_0\cos(\omega t)$, is applied to the bare metallic wire, neglecting the convection and radiation heat loss, the heat conduction equation along the metallic wire is written as

$$\frac{1}{\alpha_\mathrm{h}}\frac{\partial \Delta T_\mathrm{h}}{\partial t} - \frac{\partial^2 \Delta T_\mathrm{h}}{\partial x_\mathrm{h}^2} = \frac{2I^2 R_\mathrm{e}}{\lambda_\mathrm{h} l_\mathrm{h} S_\mathrm{h}} \cos^2(\omega t), \tag{2}$$

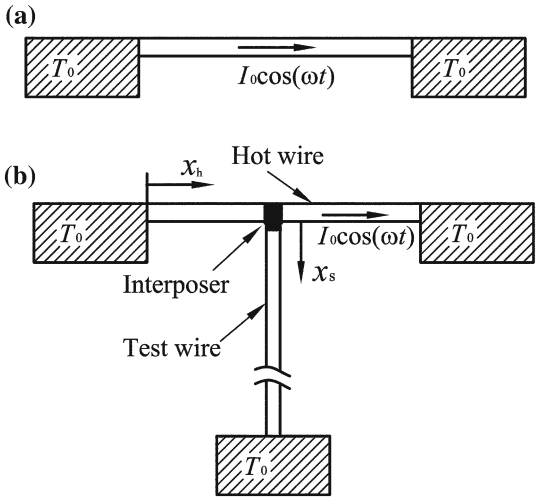

Fig. 1 Schematics for the measurement of (a) bare hot wire and (b) quasi-steady-state T-type probe with attached test wire

where ΔT_h is the temperature variation from the initial temperature, $\Delta T_h = T_h - T_0$, R_e is the electrical resistance at T_0, I is the root-mean-square (rms) value of I_0, ω is the angular frequency of the alternating current, and λ_h, α_h, l_h, and S_h are the thermal conductivity, thermal diffusivity, length, and cross-sectional area of the hot wire, respectively. As in the classical 3ω technique, only the steady transient temperature component needs to be considered, which is in the form of $\mathrm{Re}[u_h(x)e^{i2\omega t}]$ [16]. u_h is the complex temperature oscillation, containing both the amplitude of the temperature oscillation and the phase relative to the driving current. By solving Eq. 2, the average temperature oscillation can be expressed as

$$\overline{u_h} = \frac{I^2 R_e}{l_h S_h \lambda_h \beta_h}\left[1 - \frac{2}{\sqrt{\beta_h} l_h}\tanh\left(\sqrt{\beta_h} l_h/2\right)\right], \tag{3}$$

where $\beta_h = i2\omega/\alpha_h$.

As shown in Fig. 1b, one end of the test wire is attached to the midpoint of the hot wire, and the other end is connected to another heat sink. If the heating frequency is large enough to give a thermal penetration depth [17] shorter than the length of the test wire, with the coordinate system in Fig. 1b, in the frequency domain, the heat conduction equation takes the form,

$$\frac{i2\omega}{\alpha_s} u_s - \frac{\partial^2 u_s}{\partial x_s^2} = 0, \tag{4}$$

where subscript s denotes the test sample. As detailed in Refs. [15] and [18], in this quasi-steady-state experiment, the thermal impedance of the junction is introduced to simplify the experimental data analysis, which can be equivalent to the steady-state thermal contact resistance, R_r, multiplied by a ratio function, F. Exactly, the so-called thermal impedance of the junction is the differential thermal impedance, which is nothing but the difference between the total thermal impedance with and without the presence of the interposer. Taking this thermal impedance into account, the boundary condition at the junction is given by

$$\frac{u_h\,(x_h = l_h/2) - u_s(x_s = 0)}{F R_r} = -(\lambda S)_s \left.\frac{\partial u_s}{\partial x_s}\right|_{x_s=0}, \tag{5}$$

$$2\,(\lambda S)_h \left.\frac{\partial u_h}{\partial x_h}\right|_{x_h=\frac{l_h}{2}} = (\lambda S)_s \left.\frac{\partial u_s}{\partial x_s}\right|_{x_s=0}. \tag{6}$$

Then, the average temperature oscillation of the hot wire is obtained as

$$\overline{u_h} = \frac{I^2 R_e}{\lambda_h l_h S_h \beta_h} + \frac{2I^2 R_e}{\lambda_h S_h \beta_h^{3/2} l_h^2}\left\{ e^{-\sqrt{\beta_h} l_h/2} - 1 - \left[\cosh(\sqrt{\beta_h} l_h/2) - 1\right] \times \frac{b_s S_s\left(1 - e^{-\sqrt{\beta_h} l_h/2}\right) + 2b_h S_h e^{-\sqrt{\beta_h} l_h/2}\left(1 + \sqrt{i2\omega} b_s S_s F R_r\right)}{b_s S_s \sinh(\sqrt{\beta_h} l_h/2) + 2b_h S_h \cosh(\sqrt{\beta_h} l_h/2)\left(1 + \sqrt{i2\omega} b_s S_s F R_r\right)}\right\}, \tag{7}$$

where b_h is the thermal effusivity of the hot wire, and b_s and S_s represent the thermal effusivity and the cross-sectional area of the test wire, respectively. Finally, the complex third harmonic voltage across the hot wire is obtained as

$$V_3 = \frac{1}{2} I R'_e \left[\mathrm{Re}\left(\overline{u_h}\right) - \mathrm{i}\,\mathrm{Im}\left(\overline{u_h}\right) \right], \tag{8}$$

where $R'_e = \mathrm{d}R_e/\mathrm{d}T$ at the initial temperature T_0.

The results from Eqs. 3 and 7 can be nondimensionalized by introducing two dimensionless parameters, including the dimensionless thermal transfer function [19],

$$Z = \frac{\overline{u_h}}{I^2 R_e R_h}, \tag{9}$$

where R_h is the thermal resistance of the hot wire, defined by $R_h = l_h/(\lambda_h S_h)$, and the dimensionless frequency,

$$\sigma = l_h \left(\frac{\alpha_h}{2\omega}\right)^{-1/2}, \tag{10}$$

which denotes the ratio of the hot-wire length to its thermal wavelength. Correspondingly, for the self-heating 3ω method, the dimensionless thermal transfer function is expressed as

$$Z = -\frac{\mathrm{i}}{\sigma^2}\left[1 - \frac{\sqrt{2}\,(1-\mathrm{i})}{2\sigma}\tanh\left(\frac{\sqrt{\mathrm{i}}}{2}\sigma\right)\right]. \tag{11}$$

After contacting the test wire, the relation is changed to

$$Z = -\frac{\mathrm{i}}{\sigma^2} - \frac{2\sqrt{\mathrm{i}}}{\sigma^3} \times \left\{ \mathrm{e}^{-\frac{\sqrt{\mathrm{i}}}{2}\sigma} - 1 - \left[\cosh\left(\frac{\sqrt{\mathrm{i}}}{2}\sigma\right) - 1\right] \frac{1 + (2\chi S - 1)\,\mathrm{e}^{-\frac{\sqrt{\mathrm{i}}}{2}\sigma}}{\sinh\left(\frac{\sqrt{\mathrm{i}}}{2}\sigma\right) + 2\chi S \cosh\left(\frac{\sqrt{\mathrm{i}}}{2}\sigma\right)} \right\}, \tag{12}$$

where the dimensionless thermal impedance, χ, is expressed as

$$\chi = \frac{b_h}{b_s} + (\mathrm{i}+1)\frac{\sqrt{2}}{2}\frac{\sigma}{S}\frac{F R_r}{R_h}, \tag{13}$$

and $S = S_h/S_s$. Compared with the result from Eq. 11, Eq. 12 introduces another parameter χ, which contains information about the thermal effusivity of the test wire and the thermal impedance of the junction.

After calibrating the thermal properties of the hot wire using the self-heating 3ω method, the thermal effusivity of the test wire as well as the thermal impedance of the

interposer can be both obtained by a least-squares fit to give the best match between the experimental and theoretical results. Theoretically, the results obtained by fitting to the amplitude of Z using Eq. 12 and to the real and imaginary parts of χ using Eq. 13 should be consistent with each other. To evaluate the characteristic of the thermal impedance, if F is frequency independent, as shown in Eq. 13, χ is expected to vary linearly with σ, which can be conveniently applied to our experimental data analysis.

2.2 Interstitial Material

In the T-type probe, the test wire is attached to the midpoint of the hot wire using an interposer. Theoretical analysis [15] shows that the thermal impedance of the interposer in the 3ω experiment was different from its steady-state thermal resistance, as in the above discussion, a complex ratio function, F, is introduced. When the interposer is taken to be a cylinder with an idealized thickness, δ_{i}, F will depend on two dimensionless ratios,

$$E = \frac{b_{\mathrm{i}} S_{\mathrm{i}}}{b_{\mathrm{s}} S_{\mathrm{s}}} \tag{14}$$

and

$$L_{\mathrm{i}} = \delta_{\mathrm{i}} \left(\frac{\alpha_{\mathrm{i}}}{2\omega} \right)^{-1/2}, \tag{15}$$

where L_{i} denotes the ratio of the idealized thickness of the interposer to its thermal wavelength, E is the ratio of the thermal effusivity multiplying the cross-sectional area of the interposer to that of the test wire, and subscript i denotes the interposer. When these two dimensionless ratios are much smaller than 1, F approaches the upper limit of 1, in which case the thermal impedance of the interposer is equivalent to its steady-state thermal resistance. Figure 2 shows the real and imaginary parts of F as

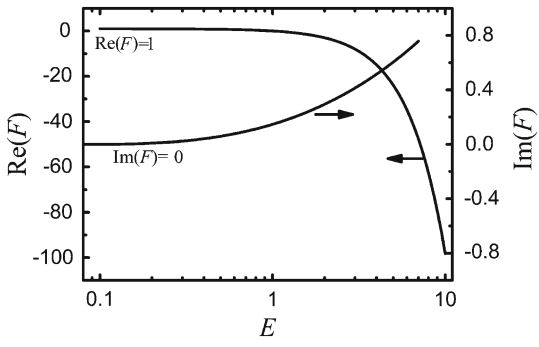

Fig. 2 Dependence of the ratio functions on E. If $E << 1$, the real part of the ratio function approaches its upper limit of 1

a function of E when $L_i = 0.001$. It is found that the real part becomes negative when $E > 1$, correspondingly, both the real and imaginary parts of χ in Eq. 13 will be inversely proportional to σ.

2.3 Radiation Effect

In the discussion above, the radial heat loss from both the hot wire and test wire is neglected. The effect of the radiation heat loss from the hot wire is insignificant, because: (1) high polished Pt wire is used as the thermometer, and the emissivity is lower than 0.1 [17], Lu et al. [20] showed that the radiation heat loss has negligible effect on the hot-wire calibration; and (2) as a thermal comparator, the same hot wire is used in the calibrating procedure and in the measurement with the test wire, the radiation heat loss can be assumed to be the same, and its effect can be further eliminated.

Comparatively, the radiation heat loss from the test wire has a more significant effect. The radiation heat loss per unit length from a cylindrical rod with diameter, D_s, is expressed as

$$q = \pi \varepsilon_s \zeta D_s \left(T_s^4 - T_0^4\right) \approx 4\pi \varepsilon_s \zeta T_0^3 D_s \Delta T_s, \tag{16}$$

where $\zeta = 5.67 \times 10^{-8}\,\mathrm{W \cdot m^{-2} \cdot K^{-4}}$ is the Stefan–Boltzmann constant, ε_s is the emissivity, and T_0 is the initial temperature. After contacting the test wire, the dimensionless thermal transfer function, Z, has the same form as in Eq. 12, but the dimensionless thermal impedance, χ, should be replaced by

$$\chi = \left(\frac{b_s^2}{b_h^2} - \mathrm{i}\frac{8\varepsilon_s \zeta T_0^3 \lambda_s}{\omega D_s b_h^2}\right)^{-1/2} + (1+\mathrm{i})\frac{\sqrt{2}}{2}\frac{\sigma}{S}\frac{F R_r}{R_h}, \tag{17}$$

where λ_s is the thermal conductivity of the test wire. The radiation heat loss contributes to the imaginary part in the first parentheses of Eq. 17, which increases continuously with decreasing angular frequency and the diameter of the test wire. Assuming that the current frequency is 0.1 Hz, the test wire is 50 μm in diameter and has the properties of Pt, the real part in the first parentheses will be 15 times larger than the imaginary part at room temperature, and the relative difference of the amplitude of χ obtained from Eqs. 13 and 17 will be less than 0.5 %, even when ε_s is taken to be 0.5. In such case, the effect of the radiation heat loss of the test wire can also be ignored.

2.4 Effect of Junction Position

If the test wire does not contact the hot wire at its midpoint, but has an offset, δ_h, the thermal transfer function in Eq. 12 is then changed to

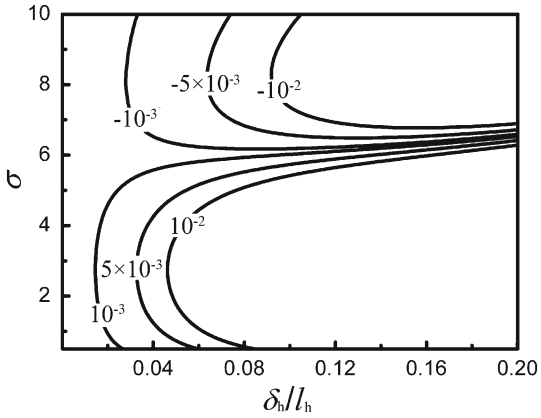

Fig. 3 Relative difference of the amplitude of the thermal transfer function, $(|Z_{\text{offset}}| - |Z|)/|Z|$, due to the departure of the junction position from the midpoint of the hot wire, with respect to the dimensionless offset ratio, δ_h/l_h, and the dimensionless frequency, σ

$$Z_{\text{offset}} = -\frac{\mathrm{i}}{\sigma^2} - \frac{\sqrt{\mathrm{i}}}{\sigma^3}\mathrm{e}^{\sqrt{\mathrm{i}}}\left\{\mathrm{e}^{-\sigma_1} + \mathrm{e}^{-\sigma_2} - 2\mathrm{e}^{-\sqrt{\mathrm{i}}} - \frac{\cosh(\sigma_2) - \mathrm{e}^{-\sqrt{\mathrm{i}}}}{\sinh(\sigma_2)}\left(\mathrm{e}^{-\sigma_1} - \mathrm{e}^{-\sigma_2}\right)\right.$$
$$-\left[\cosh(\sigma_1) + \sinh(\sigma_1)\coth(\sigma_2) - \left(\frac{\sinh(\sigma_1)}{\sinh(\sigma_2)} + 1\right)\mathrm{e}^{-\sqrt{\mathrm{i}}}\right]$$
$$\left.\times \frac{\mathrm{e}^{-\sqrt{\mathrm{i}}} - \mathrm{e}^{-\sigma_1} + \left[\mathrm{e}^{-\sigma_1} + \mathrm{e}^{-\sigma_2} - \left(\mathrm{e}^{-\sigma_1} - \mathrm{e}^{-\sigma_2}\right)\coth(\sigma_2)\right]\chi S}{\sinh(\sigma_1) + [\cosh(\sigma_1) + \coth(\sigma_2)\sinh(\sigma_1)]\chi S}\right\}, \tag{18}$$

where the lengths of the two sections of the hot wire separated by the junction are nondimensionalized as $\sigma_1 = \sigma(0.5 + \delta_h/l_h)$ and $\sigma_2 = \sigma(0.5 - \delta_h/l_h)$. Neglecting the radiation heat loss, the dimensionless thermal impedance, χ, is expressed by Eq. 13. If $\delta_h = 0$, Eq. 18 is reduced to Eq. 12.

When both the thermal impedance and the radiation heat loss from the test wire are neglected, and a 30 μm diameter Pt wire is used to measure another 50 μm Pt wire, χ will be 1 based on Eq. 17. The relative difference of the amplitude of the thermal transfer function, obtained from Eqs. 12 and 18, $(|Z_{\text{offset}}| - |Z|)/|Z|$, is plotted as a function of σ and δ_h/l_h, as shown in Fig. 3. With the utilized frequency range of 0.1 Hz to 1 Hz, σ ranges from 2 to 7. From Fig. 3, it is found that, in the case of σ lower than about 6, the amplitude of the thermal transfer function is larger when the junction is centered, and the reverse holds true for frequencies larger than 0.7 Hz. With the same frequency, the relative difference increases with increasing δ_h, and an offset ratio less than 5 % is needed to keep the relative difference within 1 %.

3 Experimental

3.1 Measurement of Pt Wire

To estimate the different characteristic of the thermal impedance at the junction, the thermal effusivity of a 50 μm diameter Pt wire is measured using two kinds of

interposers: platinum black and Apiezon N high vacuum grease. Platinum black is a solidified fine powder, which was manufactured by Ishifuku Metal Industry Corporation in Japan; and the average grain diameter is about 0.5 μm, with a purity over 99.9 %. The previous study [13] indicates that platinum black has a relatively high thermal conductivity, resulting in a negligible thermal contact resistance and a large thermal penetration depth, i.e., a small L_i. Apiezon N is a lubricating grease, which can be used in a vacuum environment down to 10^{-7} Pa and be easily removed by petroleum ether. The thermal effusivity of Apiezon N is about $630\,\mathrm{J\cdot m^{-2}\cdot K^{-1}\cdot s^{-0.5}}$(thermal conductivity of $0.194\,\mathrm{W\cdot m^{-1}\cdot K^{-1}}$, relative density of 0.911, and specific heat of $2.25\times10^3\,\mathrm{J\cdot kg^{-1}\cdot K^{-1}}$) [21], much lower than that of the metallic materials. For the utilized current frequency range of 0.1 Hz to 1 Hz, the corresponding thermal wavelength of Apiezon N ranges from 270 μm to 85 μm.

In the measurement, another Pt wire (diameter of 30 μm, length of 9 mm) is used as the hot wire, the temperature coefficient of resistance is calibrated to be $0.0037\,\mathrm{K^{-1}}$. A Labview-based virtual lock-in is used to detect both the third harmonic voltage and the first harmonic voltage across the hot wire with a 24-bit flexible resolution digitizer. Additional details about the measurement system can be found in Ref. [14].

Figure 4 shows the dependence of the dimensionless thermal impedance on the dimensionless frequency. For the platinum black contact, Im(χ) is negative and decreases with increasing σ, while a positive slope is obtained for the Apiezon N contact. With the theoretical prediction using Eq. 13, the best-fit thermal effusivity and the thermal impedance of the interposer are found to be $1.40\times10^4\,\mathrm{J\cdot m^{-2}\cdot K^{-1}\cdot s^{-0.5}}$ and $3660\,\mathrm{K\cdot W^{-1}}$ for the Apiezon N contact. Using the platinum black contact, the corresponding results are $1.36\times10^4\,\mathrm{J\cdot m^{-2}\cdot K^{-1}\cdot s^{-0.5}}$ and $-3250\,\mathrm{K\cdot W^{-1}}$, respectively. It is interesting to find that a similar thermal effusivity of the test wire is obtained using both interposers, so the ratio function, F, can be verified to be frequency independent for both cases. The obtained negative thermal impedance for the platinum black contact can be explained by a comparison of the average temperature oscillation of the hot wire with and without the interposer, if $E > 1$, the former is larger than the latter.

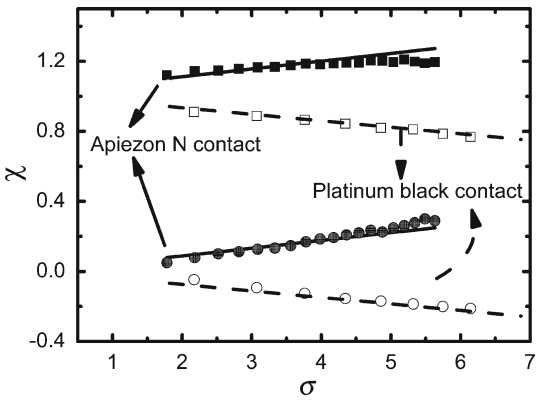

Fig. 4 Dimensionless thermal impedance [(■) and (•) denote Re(χ) and Im(χ) with the Apiezon N contact, (□) and (○) denote Re(χ) and Im(χ) with the platinum black contact] with respect to the dimensionless frequency. The fitted curves represent theoretical predictions from Eq. 13

3.2 Measurement of Thermal Contact Resistance

From Fig. 2, if the ratio function, F, approaches the upper limit of 1, the quasi-steady-state method would offer a novel way to determine the thermal contact resistance, in which case the interposer with high thermal conductivity cannot be applied, and the low thermal effusivity grease is preferred.

For the measurement of the previous Pt wire, the thermal impedance of the Apiezon N contact is less than $4000\,\mathrm{K}\cdot\mathrm{W}^{-1}$. Comparatively, using the conventional steady-state T-type probe [10], the thermal resistance of the test Pt wire is determined to be about $1.71\times10^{5}\,\mathrm{K}\cdot\mathrm{W}^{-1}$; thus, the thermal impedance has a negligible effect on the thermal-conductivity measurement, and the thermal conductivity of the Pt wire is found to be $72.0\,\mathrm{W}\cdot\mathrm{m}^{-1}\cdot\mathrm{K}^{-1}$. To confirm the assumption that the thermal impedance of the interposer with low effusivity has a similar behavior to the steady-state contact resistance [15], a 100 μm Cu wire is measured using the same experimental system with the Apiezon N contact. Figure 5a shows the dimensionless thermal impedance as a function of the dimensionless frequency; the fitted thermal effusivity and thermal impedance are $3.40\times10^{4}\,\mathrm{J}\cdot\mathrm{m}^{-2}\cdot\mathrm{K}^{-1}\cdot\mathrm{s}^{-0.5}$ and $9500\,\mathrm{K}\cdot\mathrm{W}^{-1}$, respectively. The experimental result obtained from the steady-state T-type probe is

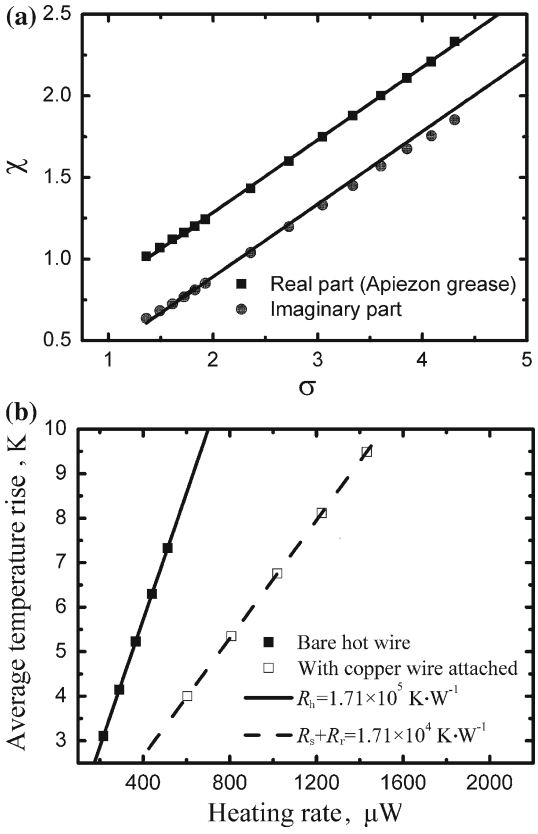

Fig. 5 Experimental results for a Cu wire using Apiezon N as the interposer, (a) dependence of Re(χ) and Im(χ) on the dimensionless frequency, the solid lines are the least-squares fit using Eq. 13; and (b) thermal conductivity measurement using the steady-state T-type probe, the total thermal resistance introduced by the attached Cu wire is found to be $1.71\times10^{4}\,\mathrm{K}\cdot\mathrm{W}^{-1}$

shown in Fig. 5b. The total thermal resistance introduced by the attached Cu wire is $1.71 \times 10^4\,\mathrm{K \cdot W^{-1}}$; the diameter of the Cu wire is measured to be 96.6 μm using the scanning electron microscope, and the length is found to be 22.86 mm using an optical microscope with a resolution of 0.02 mm. If the thermal impedance of the junction is neglected, the thermal conductivity of the Cu wire is calculated to be $182\,\mathrm{W \cdot m^{-1} \cdot K^{-1}}$, much smaller than the reference value [17]. After substituting the thermal impedance obtained from the quasi-steady-state measurement, the intrinsic thermal resistance of the Cu wire is determined to be about $7600\,\mathrm{K \cdot W^{-1}}$, leading to a thermal conductivity of $410\,\mathrm{W \cdot m^{-1} \cdot K^{-1}}$. Compared with the reference value of $401\,\mathrm{W \cdot m^{-1} \cdot K^{-1}}$, a relatively large value is obtained, which can be explained by the effect of the radiation heat loss on the steady-state measurement [22].

4 Conclusions

The characteristic of the thermal impedance of the junction in a quasi-steady-state T-type probe was investigated using two kinds of interposers, including solidified platinum black and Apiezon N grease. Measurements on a Pt wire showed that the platinum black contact exhibited an expected negative thermal impedance, while a positive thermal impedance was obtained for the Apiezon N contact, and both results were fitted well with the experimental data. The measurement was then extended to a Cu wire, in which case the thermal contact resistance had a non-negligible effect on the heat transport, and the thermal impedance of the interposer in this quasi-steady-state experiment was verified to be equivalent to its steady-state thermal resistance, under the conditions that the interposer is thermally thin, and the thermal effusivity multiplying the cross-sectional area of the interposer is smaller than that of the test wire.

Acknowledgments This work was supported by the National Natural Science Foundation of China (Grant Nos. 50676046 and 50730006).

References

1. D.G. Cahill, K.E. Goodson, A. Majumdar, J. Heat Transf. **124**, 223 (2002)
2. P. Kim, L. Shi, A. Majumdar, P.L. McEuen, Phys. Rev. Lett. **87**, 215502 (2001)
3. C. Yu, S. Saha, J. Zhou, L. Shi, A.M. Cassell, B.A. Cruden, Q. Ngo, J. Li, J. Heat Transf. **128**, 234 (2006)
4. C.W. Chang, D. Okawa, H. Garcia, A. Majumdar, A. Zettl, Phys. Rev. Lett. **101**, 075903 (2008)
5. S.-M. Lee, D.G. Cahill, J. Appl. Phys. **81**, 2590 (1997)
6. Z.L. Wang, D.W. Tang, W.G. Zhang, J. Phys. D: Appl. Phys. **40**, 4686 (2007)
7. O.W. Kading, H. Skurk, K.E. Goodson, Appl. Phys. Lett. **65**, 1629 (1994)
8. H.K. Lyeo, D.G. Cahill, Phys. Rev. B **73**, 144301 (2006)
9. V.V. Deshpande, S. Hsieh, A.W. Bushmaker, M. Bockrath, S.B. Cronin, Phys. Rev. Lett. **102**, 105501 (2009)
10. X. Zhang, S. Fujiwara, M. Fujii, Int. J. Thermophys. **21**, 965 (2000)
11. M. Fujii, X. Zhang, H.Q. Xie, H. Ago, K. Takahashi, T. Ikuta, H. Abe, T. Shimizu, Phys. Rev. Lett. **95**, 065502 (2005)
12. C. Dames, S. Chen, C.T. Harris, J.Y. Huang, Z.F. Ren, M.S. Dresselhaus, G. Chen, Rev. Sci. Instrum. **78**, 104903 (2007)

13. J.L. Wang, M. Gu, X. Zhang, Y. Song, J. Phys. D: Appl. Phys. **42**, 105502 (2009)
14. J.L. Wang, M. Gu, X. Zhang, G.P. Wu, Rev. Sci. Instrum. **80**, 076107 (2009)
15. J.L. Wang, M. Gu, X. Zhang, G.P. Wu (unpublished)
16. H.S. Carslaw, J.C. Jaeger, *Conduction of Heat in Solids*, 2nd edn. (Oxford University Press, London, 1959), p. 65
17. F.P. Incropera, D.P. Dewitt, T.L. Bergman, A.S. Lavine, *Fundamentals of Heat and Mass Transfer*, 2nd edn. (Wiley, New York, 2007), p. A-3
18. T. Tong, A. Majumdar, Rev. Sci. Instrum. **77**, 104902 (2006)
19. C. Dames, G. Chen, Rev. Sci. Instrum. **76**, 124902 (2005)
20. L. Lu, W. Yi, D.L. Zhang, Rev. Sci. Instrum. **72**, 2996 (2001)
21. Apiezon N Cryogenic High Vacuum Grease, data sheet, August 2005
22. M. Gu, *Thermal Conductivity Measurement of an Individual Carbon Fiber by Modified T-Type Method* (M. S. Thesis, Tsinghua University, Beijing, China, 2009), pp. 40–47